

Spontaneous Formation of Altermagnetism from Orbital Ordering

Valentin Leeb,^{1,2} Alexander Mook,³ Libor Šmejkal,^{3,4} and Johannes Knolle^{1,2,5}

¹Technical University of Munich, TUM School of Natural Sciences,
Physics Department, TQM, 85748 Garching, Germany

²Munich Center for Quantum Science and Technology (MCQST), Schellingstr. 4, 80799 München, Germany

³Institut für Physik, Johannes Gutenberg Universität Mainz, D-55099 Mainz, Germany

⁴Institute of Physics, Czech Academy of Sciences, Cukrovarnická 10, 162 00 Praha 6 Czech Republic

⁵Blackett Laboratory, Imperial College London, London SW7 2AZ, United Kingdom

(Dated: December 19, 2023)

Altermagnetism has emerged as a third type of collinear magnetism. In contrast to standard ferromagnets and antiferromagnets, altermagnets exhibit extra even-parity wave spin order parameters resulting in a spin-splitting of electronic bands in momentum space. In real space, sublattices of opposite spin polarization are anisotropic and related by rotational symmetry. In the hitherto identified altermagnetic candidate materials the anisotropies arise from the local crystallographic symmetry. Here, we show that altermagnetism can also form as an interaction-induced electronic instability in a lattice without the crystallographic sublattice anisotropy. We provide a microscopic example of a two-orbital model showing that the coexistence of staggered antiferromagnetic and orbital order can realize robust altermagnetism. We quantify the spin-splitter conductivity as a key experimental observable and discuss material candidates for the interaction-induced realization of altermagnetism.

Introduction.— The interplay of competing orders from strong electronic correlations gives rise to rich phase diagrams of quantum materials, for example, nematic or antiferromagnetic (AFM) order in the vicinity of superconductivity [1]. When different orders coexist, qualitatively new behavior can emerge that is not present in the individual phases. For example, superconductivity in materials with long-range magnetism can realize unconventional finite momentum pairing [2, 3]. Here, we show that electron correlations can give rise to a phase with coexisting staggered orbital order (OO) and Néel antiferromagnetism (AFM), which spontaneously realizes a *d*-wave altermagnetic phase with spin-polarized electronic bands and a large transverse spin conductivity.

Recently, altermagnetism has been delimited with the help of spin symmetries as a third type of collinear magnetism [4]. Similar to standard AFM, an altermagnet displays long-range order with zero net magnetization, e.g. realized by the presence of two sublattices with opposite spin alignment. However, in contrast to usual AFM the Néel vector is not sufficient for describing an altermagnet because it exhibits an extra even-parity wave order parameter [4–12]. The extra *d*, *g*, *i*-wave spin order takes in momentum space a form of unconventional spin-splitting of the electronic band structure [4, 6, 7, 10] which has recently been confirmed experimentally in photoemission experiments in MnTe [10, 13]. In real space, altermagnets are characterized by anisotropies of spin sublattices, which is best explained with the example of a *d*-wave state on a square lattice, see left column of Fig. 1. With crystallographic anisotropies, e.g. asymmetric ligands on the bonds, the unit cell has two sites and as a result, in the magnetic state a flip of all spins is not equivalent to a translation or inversion operation between the spin sublattices but instead they are related by an additional real space rotation [4].

So far, research on altermagnets has concentrated on systems where the crystal structure imprints an anisotropic spin density and the two sublattices are globally inequivalent even in the non-magnetic high-temperature phase [4–8, 11] as in

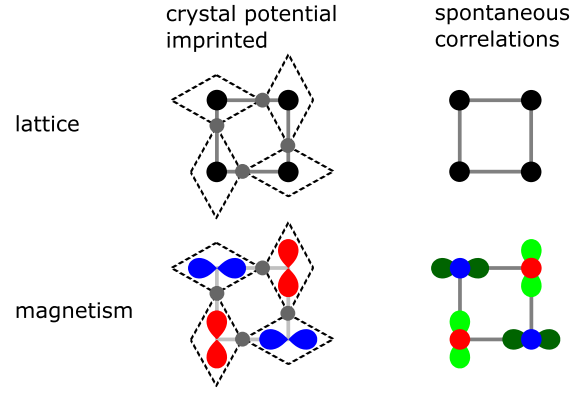


FIG. 1. Comparison of the established crystal potential-imprinted altermagnetism (left column) and altermagnetism due to spontaneous correlations (right column) on a square lattice. For the former, the crystal structure provides a two site unit cell whose sublattices are related only by rotation but not by inversion symmetry or translation. The symmetry of the lattice, typically due to non-magnetic ions (grey vertices), is imprinted on the electronic density leading to anisotropic spin densities (red, blue) in the magnetically ordered state (lower left). In contrast, for spontaneous altermagnetism the lattice is isotropic and the crucial symmetry lowering happens spontaneously due to a staggered orbital ordering (green).

the above example. Below the transition temperature it is then the crystal structure which modulates the spin density into an anisotropic shape with opposite spin channels related by crystal rotations or mirrors (possibly non-symmorphic). Although there is an increasing number of materials of this type, metallic altermagnets are currently rare, and it remains an open question whether altermagnetism can be realized spontaneously via electronic correlations [14]? Here, we provide an affirmative answer and demonstrate how altermagnetism can be realized as an OO transition. We concentrate on a minimal two orbital model of transition metal systems with directional

$d_{xz/yz}$ orbitals. Crucially, altermagnetism emerges as a *spontaneous* electronic instability in a model whose crystal structure has globally equivalent sublattices, i.e. the lattice does not exhibit the local crystallographic anisotropies. Instead, it is the staggered (π, π) -OO coexisting with (π, π) -AFM, see right column in Fig. 1, which leads to the anisotropic spin sublattices, which are again related by rotational symmetry. We also show that our proposed mechanism can generate a strong spin-splitter effect, i.e. a transverse spin-polarized current with spin d -wave symmetry [15, 16] controlled by the OO.

The example of a d -wave altermagnet has been known for some time [5, 17] as the magnetic-analogue of d -wave superconductivity [18]. In a long-wavelength momentum space description it can arise as a spin-triplet Pomeranchuk instability of an interacting Fermi liquid, however no realistic candidates have been identified [14]. Here, we show a realization of the d -wave altermagnetic state in a microscopic lattice model of transitional metal systems with non-trivial orbital degrees of freedom, which alludes the real space symmetry properties of altermagnetism. In this context it is interesting to note that the dichotomy between a weak coupling momentum space instability compared to a real space OO instability is similar to the case of Ising nematic order observed in parent compounds of iron-based superconductors [19]. There, the breaking of the lattice rotational symmetry can be either understood as a Fermi surface type instability [20] or a spontaneous OO transition from local Hubbard type interactions [21–23]. Both describe similar physics but while the former approach concentrates on the universal aspects the latter takes into account microscopic details of a given material. Similarly, we show that our microscopic real space description highlights the role of orbital degrees of freedom for realizing d -wave altermagnetism from the coexistence of AFM and staggered OO, which allows us to identify a number of possible materials candidates such as perovskites, square pnictides, and vanadates, which we discuss in the outlook section.

Two orbital model.— We concentrate on a minimal model of interacting electrons on the square lattice. The full Hamiltonian is given by $H = H_0 + H_J + H_V$. The kinetic part H_0 consists of two orbitals of the d_{xz} and d_{yz} type described by

$$H_0 = \sum_{\mathbf{k}, s} \Psi_{\mathbf{k}s}^\dagger \begin{pmatrix} \varepsilon_x(\mathbf{k}) & \varepsilon_{xy}(\mathbf{k}) \\ \varepsilon_{xy}(\mathbf{k}) & \varepsilon_y(\mathbf{k}) \end{pmatrix} \Psi_{\mathbf{k}s} \quad (1)$$

with

$$\varepsilon_x(\mathbf{k}) = -2t_1 \cos k_x - 2t_2 \cos k_y - 4t_3 \cos k_x \cos k_y, \quad (2)$$

$$\varepsilon_y(\mathbf{k}) = -2t_2 \cos k_x - 2t_1 \cos k_y - 4t_3 \cos k_x \cos k_y, \quad (3)$$

$$\varepsilon_{xy}(\mathbf{k}) = -4t_4 \sin k_x \sin k_y. \quad (4)$$

and the components $\Psi_{\mathbf{k}\alpha s} = 1/\sqrt{N} \sum_j e^{i\mathbf{k}\cdot\mathbf{r}_j} \Psi_{j\alpha s}$ of the vector $\Psi_{\mathbf{k}}$ annihilate an electron with momentum \mathbf{k} and spin s in orbital α . N is the number of sites and \mathbf{r}_j the coordinate of the j th unit cell. For concreteness, we fix $t_1 = -t$, $t_2 = -1.75t$, $t_3 = -0.85t$, $t_4 = -0.65t$ throughout this work. The anisotropy of the orbitals is imprinted in the hoppings, e.g. t_1 quantifies d_{xz} to d_{xz} hopping along the x -direction and d_{yz} to d_{yz} hopping along the y -direction and t_2 d_{xz} (d_{yz}) to d_{xz} (d_{yz}) hopping along

the $y(x)$ -direction. The remaining allowed overlaps are the intraorbital next-nearest neighbor term t_3 , and t_4 as a phase changing interorbital next-nearest neighbor hopping, see the Supplementary Material (SM) for a visualization [24]. The model has been proposed previously as a minimal model for iron-pnictides [25] but can be adapted to describe any transition metal materials with dominating d_{xz}/d_{yz} orbital contributions.

A natural choice for the interactions would be the local form of the Coulomb repulsion in the Kanamori form [26] including on-site Hubbard interactions, FM exchange from Hund's coupling, as well as inter-orbital density repulsion and pair hopping [25, 27, 28]. However, the precise value of the interactions are in general hard to quantify and longer range components of the interaction are neglected. Moreover, many different competing phases can be induced by the interactions depending on the precise form of the Fermi surface. To avoid complications from other competing states, and as a proof of principle, we chose to concentrate on the following effective interactions

$$H_J = J \sum_{\langle ij \rangle} \mathbf{S}_i \cdot \mathbf{S}_j \quad \text{and} \quad H_V = V \sum_{\langle ij \rangle} N_i^z N_j^z, \quad (5)$$

with $S_i^\nu = \Psi_i^\dagger \underline{S}^\nu \otimes \mathbb{1} \Psi_i$ the total spin at site i . The first term is a usual AFM Heisenberg exchange and the second term with $N_i^z = \Psi_i^\dagger \mathbb{1} \otimes \underline{\alpha}^z \Psi_i = \sum_s \Psi_{ixs}^\dagger \Psi_{ixs} - \Psi_{iys}^\dagger \Psi_{iys}$ is an Ising type interaction between the nearest neighbor on-site relative orbital densities. We denote the Pauli matrix (component ν) for the spin (orbital) subspace by \underline{S}^ν ($\underline{\alpha}^\nu$). We then expect that H_J induces (π, π) -AFM and, crucially, H_V induces (π, π) -OO. Because of the absence of spin-orbit coupling, $[H, S_i^\nu] = 0$ and the spin remains a good quantum number. Note however, that this is not true for the orbital character, because t_4 couples the d_{xz} and d_{yz} orbitals.

Phase diagram.— Next, we study the full Hamiltonian in a Hartree-Fock mean-field approximation. In our ansatz, we focus on (π, π) instabilities and introduce two sublattices $\lambda = A, B$ of even and odd sites. The fermions $\Psi_{\mathbf{k}\alpha\lambda s}$ of the eight component vector $\Psi_{\mathbf{k}}$ get the new quantum number λ and analogously to above $\underline{\lambda}^\nu$ is the Pauli- ν matrix acting in the sublattice subspace. We can then define the mean fields $\delta m = \sum_i (-1)^i \langle S_i^z \rangle / N$, i.e. the order parameter for the staggered AFM, and $\delta n = \sum_i (-1)^i \langle N_i^z \rangle / N$, the order parameter for staggered OO. Decoupling the Hamiltonian in the charge channel, we find

$$H_J/16J = -\delta m \sum_{\mathbf{k}} \Psi_{\mathbf{k}}^\dagger \underline{S}^z \otimes \underline{\lambda}^z \otimes \mathbb{1} \Psi_{\mathbf{k}} + 4\delta m^2, \quad (6)$$

$$H_V/16V = -\delta n \sum_{\mathbf{k}} \Psi_{\mathbf{k}}^\dagger \mathbb{1} \otimes \underline{\lambda}^z \otimes \underline{\alpha}^z \Psi_{\mathbf{k}} + 4\delta n^2. \quad (7)$$

The resulting mean-field Hamiltonian $H = \sum_{\mathbf{k}} \Psi_{\mathbf{k}}^\dagger h(\mathbf{k}) \Psi_{\mathbf{k}} + E_0$, see SM [24], is a non-interacting Hamiltonian, hence the 8×8 Bloch Hamiltonian $h(\mathbf{k})$ can be efficiently diagonalized for each momentum to obtain the eigenenergies $\epsilon_m(\mathbf{k})$ and the Bloch eigenstates $|u_m(\mathbf{k})\rangle$ with band index m . Note that H is block-diagonal in spin, but in contrast to the conventional

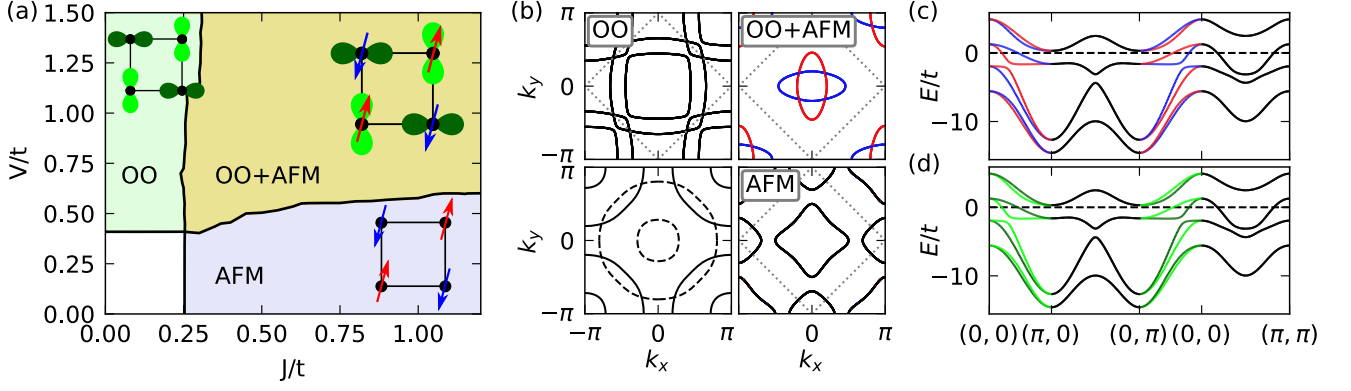


FIG. 2. Mean-field phase diagram and electronic structure of the model Hamiltonian. (a) Zero-temperature mean-field phase diagram for filling $n = 5.7216$. There is a trivial phase (white), a phase with (π, π) -antiferromagnetic order (AFM, light blue), a phase with a (π, π) -orbital ordered state (OO, light green), and an altermagnetic phase where AFM and OO are present simultaneously (OO+AFM, ocher). (b) Representative Fermi surfaces of each phase in the crystallographic Brillouin zone. The bands' spin character $\langle s^z \otimes \mathbb{1} \otimes \mathbb{1} \rangle$ is indicated by color, with red/blue/black denoting spin-up/spin-down/spin-degenerate. The magnetic Brillouin zone is indicated by gray dotted lines and the dashed contours in the lower left panel (trivial phase) indicate the additional part of the Fermi surface that is present when working in the magnetic $\sqrt{2} \times \sqrt{2}$ unit cell. (c) The electronic band structure along high-symmetry directions in the OO+AFM phase. The bands are both spin-polarized [upper panel, coloring as in (b)] and orbital-polarized (lower panel). Darkgreen (lightgreen) coloring indicates d_{xz} (d_{yz}) orbital character ($\mathbb{1} \otimes \mathbb{1} \otimes \alpha^z$) and black degeneracy. A $\pi/2$ rotation, which maps the $(0, 0) - (0, \pi)$ path onto the $(0, 0) - (\pi, 0)$ path, also maps oppositely spin- and orbital-polarized bands onto each other.

AFM spin density mean-field solution [29] the two blocks are explicitly spin-dependent. We have solved the mean-field equations self-consistently for fixed filling n by iteration, i.e. we calculated δm_i and δn_i from $H(\delta m_{i-1}, \delta n_{i-1})$ until convergence, defined by $|\delta m_i - \delta m_{i-1}|, |\delta n_i - \delta n_{i-1}| < 10^{-3}$, was reached.

The resulting phase diagram features four different metallic phases, see Fig. 2 (a). For dominating Heisenberg exchange, i.e. J/t larger than roughly 0.25 and small V , AFM order develops as expected. Conversely, for dominating orbital repulsion between nearest neighbor sites, i.e. V/t larger than 0.5 and small J , OO develops. Crucially, we also find a large coexistence regime (OO+AFM). Importantly, because of the staggered OO the two sublattices of up and down spins are only connected by a real space rotation taking $d_{xz} \rightarrow d_{yz}$, but not by translation or inversion as is the case in the pure AFM phase.

The spontaneous symmetry breaking in the OO+AFM phase has important consequences for the electronic structure. Figures 2 (b,c) show that only in the coexistence OO+AFM phase the spin degeneracy of the bands is removed, as is evidenced by a spin-split Fermi surface (red for spin up and blue for spin down). As expected for the altermagnetic phase, the spin polarized bands are related by $\pi/2$ rotations in momentum space. As an interesting side note, we also find that within our two-orbital only model, the bands are also perfectly orbital polarized as shown in the lower panel of Fig. 2 (c).

Spin conductivity.— Next, we study the unique experimental signatures of the OO+AFM coexistence phase. One of the key features of d -wave altermagnets is the appearance of a longitudinal spin conductivity without magnetization and a spin-splitter effect [15]. The anisotropic spin-polarized Fermi

surfaces respond to electric fields by generating characteristic spin currents, see Fig. 2 (b). When the field is applied in the [100] direction (x direction), the spin-up polarized Fermi surface contributes stronger to transport than the spin-down polarized Fermi surface. As a result, the spin-polarized currents j_\uparrow and j_\downarrow per Fermi surface are unequal aligned and there is a net spin-polarized current in direction of the electric field.

To quantify the spin current strength, we evaluate the conductivity along the crystal axis, given in its most general form by the Kubo formula [15]

$$\sigma_{bc}(O^a) = -\frac{e\pi}{N} \sum_{\mathbf{k}, n, m} A_n(\mathbf{k}, \omega) \langle u_n(\mathbf{k}) | J_b(O^a, \mathbf{k}) | u_m(\mathbf{k}) \rangle \times A_m(\mathbf{k}, \omega) \langle u_m(\mathbf{k}) | v_c(\mathbf{k}) | u_n(\mathbf{k}) \rangle. \quad (8)$$

Here, $A_n(\mathbf{k}, \omega) = \frac{1}{\pi} \frac{\Gamma}{(\omega - \epsilon_n(\mathbf{k}))^2 + \Gamma^2}$ is the band-resolved spectral function with a positive infinitesimal broadening Γ , $v_c = \partial h(\mathbf{k}) / \partial k_c$ is the velocity operator and $J_b(O^a) = \frac{1}{2} \{O^a, v_b\}$ the current operator. The summation extends over all eight bands n, m and all momenta \mathbf{k} of the magnetic Brillouin zone. Eq. (8) captures charge $\sigma^0 = \sigma(\mathbb{1})$, spin $\sigma^z = \sigma(\underline{s}^z)$ and orbital conductivity $\sigma(L^z)$ by adapting the current operator to $J_b(\mathbb{1}) = v_b$, $J_b(\underline{s}^z) = \underline{s}^z \otimes \mathbb{1} \otimes \mathbb{1} v_b$ or $J_b(L^z) = \frac{1}{2} \{\mathbb{1} \otimes \mathbb{1} \otimes L^z, v_b\}$ respectively. We show the magnitude of the respective spin-conductivity tensor element σ_{xx}^z in Fig. 3 (c). The transversal component $\sigma_{xy}^z = 0$ vanishes.

An electric field applied in the [110] direction induces non-parallel spin-currents enclosing the spin splitter angle α , see Fig. 3 (a) and (b). The spin splitter angle $\tan(\alpha/2) = |\sigma_{xx}^z / \sigma_{xx}^0|$ quantifies the strength of spin transport compared to standard charge transport and takes its theoretical maximal value of 90° for strongly anisotropic elongated Fermi pockets. As shown in

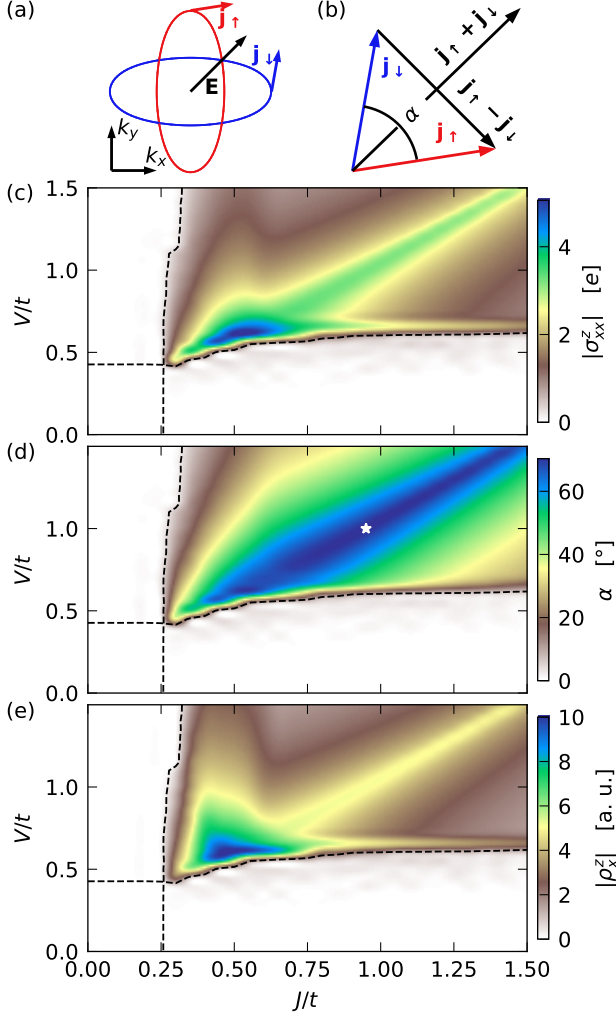


FIG. 3. Nonrelativistic spin-polarized currents in the OO+AFM altermagnetic phase. (a) The spin-split Fermi surface in the altermagnetic phase leads to a finite spin conductivity $\sigma(\underline{s}^z) = \sigma^z$, because the spin polarized Fermi surfaces respond with different currents $\mathbf{j}_\uparrow, \mathbf{j}_\downarrow$ to an external electric field \mathbf{E} . The shown Fermi surface has the maximal spin splitter angle. (b) The spin splitter angle α is the angle between the spin currents. Colorplots of the longitudinal component of the spin conductivity $\sigma_{xx}^z = -\sigma_{yy}^z$ (c), the spin splitter angle α (d) (α_{\max} indicated by star) and the directed spin density of states $\rho_x^z = -\rho_y^z$ (e). The dashed lines indicate the phase boundaries as extracted in Fig. 2 (a).

Fig. 3 (d), we find a maximal spin splitter angle $\alpha_{\max} = 70.3^\circ$ around $J = V \approx t$ for the Fermi surface shown in Fig. 3 (a).

Crucially, σ^z and α are only non-zero in the altermagnetic phase as evidenced by the spin split Fermi surface. They take the maximum values in the bulk of the OO+AFM phase where $V \approx J$. This shows that for large spin splitting it is more relevant that δm and δn are of the same size than their individual magnitudes. Unexpectedly, the spin conductivity σ^z peaks closely to the AFM phase transition throughout the entire phase diagram, see Fig. 5 in the SM.

The spin conductivity Eq. (8) is a direct result of the altermagnetic spin splitting. We can alternatively quantify the latter by studying a simpler more intuitive quantity, the spin density of states weighted with the Fermi velocity

$$\rho_b^z = \frac{1}{N} \sum_{\mathbf{k}, n} A_n(\mathbf{k}) |\partial_b \epsilon_n(\mathbf{k})| \langle u_n(\mathbf{k}) | \underline{s}^z \otimes \mathbb{1} \otimes \mathbb{1} | u_n(\mathbf{k}) \rangle. \quad (9)$$

It is numerically cheaper to compute and behaves analogously to the spin conductivity, see Fig. 3 (e). Although the spin density of states weighted with the Fermi velocity is not a direct physical observable it can be used as a simple measure to quantify spin splitting for metallic altermagnets.

Deep in the AFM+OO phase the bands are also strongly orbital polarized, see Fig. 2 (d), resembling the spin character. Therefore one might expect that our findings for the spin conductivity carry over to the orbital conductivity $\sigma(L^z)$. In order to evaluate $\sigma(L^z)$, we identify x (y) with the atomic orbitals d_{xz} (d_{yz}), and from Eq. (8) use the orbital current operator $J_b(L^z) = \frac{1}{2}(\mathbb{1} \otimes \mathbb{1} \otimes \underline{\alpha}^y, v_b)$. It turns out that the orbital conductivity vanishes exactly $\sigma(L^z) = 0$. The reason is that the bands are orbital polarized but only the superpositions $d_{xz} \pm id_{yz}$ are eigenstates of the angular momentum operator L^z . This is an artifact of our minimal two-orbital model and in the future it will be interesting to explore the orbital conductivity taking into account the full d -orbital manifold of states.

Discussion and Outlook.— We have shown that the spontaneous lattice symmetry breaking from OO in conjunction with basic Néel AFM can give rise to an altermagnetic phase with strongly spin polarized bands. In contrast to existing proposals to look for altermagnets in materials with local crystallographic sublattice anisotropies [6] our proposed mechanism of interaction-induced OO considerably broadens the range of materials candidates. Staggered OO has been experimentally observed on the surface of CeCoIn₅ [30] or famously in the perovskite-type transition-metal oxides like LaMnO₃ [31–33]. Another promising material platform are Fe-based square lattices. In fact, recently it was shown that checkerboard AFM order in FeSe subjected to an electric field can generate an altermagnetic state [34] and the same could be achieved by the presence of staggered OO.

A challenge is that most materials with staggered OO, e.g. C-type, display spin-ordering of a different type, e.g. G-type AFM or FM [35]. In fact, the tendency of staggered OO to show FM is in accordance with the well-known Goodenough-Kanamori rules [36], but in certain cases these phenomenological rules may be violated [37–39]. Perhaps the most promising candidate materials in this context are cubic vanadates [40] which have been shown to display staggered OO coexisting with AFMs [41, 42]. The precise form of the OO pattern appears even tuneable via thin film strain engineering [43] which opens the possibility for realizing the required coexistence patterns for an altermagnetic phase. Hence, in the future it will be important to explore microscopic scenarios for realistic material platforms.

Beyond the strong coupling analysis, it would also be worthwhile to start with a weak-coupling theory and microscopic interaction parameters to analyze when the AFM and

OO susceptibilities of the metallic phase diverge simultaneously. In that context, we note that our coexistence phase of AFM and OO has already been discussed as a potential instability of more generic models, e.g. see Fig. 2 (f) of Ref. [44], but a systematic study how to stabilize these is missing. Similarly, studies of the dynamical response functions in the coexistence regime will be important for making contact to scattering experiments.

In conclusion, we have shown how electronic correlations can lead to the spontaneous formation of altermagnetic phases due to OO. As this considerably broadens the range of candidate materials we hope that our work is a stepping stone for realizing new altermagnets.

DATA AND CODE AVAILABILITY

Code and data related to this paper are available on Zenodo [45] from the authors upon reasonable request.

ACKNOWLEDGMENTS

We thank M. Knap for helpful discussions and related collaborations. J. K. especially thanks K. Wohlfeld for valuable discussions and for pointing out the connection to Goodenough-Kanamori rules as well as vanadates. V. L. acknowledges support from the Studienstiftung des deutschen Volkes. J. K. acknowledges support from the Imperial-TUM flagship partnership. The research is part of the Munich Quantum Valley, which is supported by the Bavarian state government with funds from the Hightech Agenda Bayern Plus. This work is funded in part by the Deutsche Forschungsgemeinschaft (DFG, German Research Foundation) - Project No. 504261060. L. S. acknowledges support from the Johannes Gutenberg-Universität Mainz Top-Dyn initiative (project ALTERSEED), and funding from Deutsche Forschungsgemeinschaft (DFG) grant no. TRR 288 - 422213477 (Project B05).

-
- [1] E. Fradkin, S. A. Kivelson, and J. M. Tranquada, Colloquium: Theory of intertwined orders in high temperature superconductors, *Reviews of Modern Physics* **87**, 457 (2015).
 - [2] P. Fulde and R. A. Ferrell, Superconductivity in a strong spin-exchange field, *Physical Review* **135**, A550 (1964).
 - [3] A. Larkin and Y. N. Ovchinnikov, Nonuniform state of superconductors, *Soviet Physics-JETP* **20**, 762 (1965).
 - [4] L. Šmejkal, J. Sinova, and T. Jungwirth, Beyond conventional ferromagnetism and antiferromagnetism: A phase with nonrelativistic spin and crystal rotation symmetry, *Physical Review X* **12**, 031042 (2022).
 - [5] L. Šmejkal, R. González-Hernández, T. Jungwirth, and J. Sinova, Crystal time-reversal symmetry breaking and spontaneous hall effect in collinear antiferromagnets, *Science Advances* **6**, eaaz8809 (2020).
 - [6] L. Šmejkal, J. Sinova, and T. Jungwirth, Emerging research landscape of altermagnetism, *Physical Review X* **12**, 040501 (2022).
 - [7] I. Mazin, Editorial: Altermagnetism—a new punch line of fundamental magnetism, *Physical Review X* **12**, 040002 (2022).
 - [8] I. I. Mazin, K. Koepnick, M. D. Johannes, R. González-Hernández, and L. Šmejkal, Prediction of unconventional magnetism in doped fcsb2, *PNAS* **118**, e2108924118 (2021).
 - [9] Z. Feng, X. Zhou, L. Šmejkal, L. Wu, Z. Zhu, H. Guo, R. González-Hernández, X. Wang, H. Yan, P. Qin, X. Zhang, H. Wu, H. Chen, Z. Meng, L. Liu, Z. Xia, J. Sinova, T. Jungwirth, and Z. Liu, An anomalous hall effect in altermagnetic ruthenium dioxide, *Nature Electronics* **5**, 735 (2022).
 - [10] J. Krempaský, L. Šmejkal, S. W. D'Souza, M. Hajlaoui, G. Springholz, K. Uhlířová, F. Alarab, P. C. Constantinou, V. Stokov, D. Usanov, W. R. Pudelko, R. González-Hernández, A. B. Hellenes, Z. Jansa, H. Reichlová, Z. Šobán, R. D. G. Betancourt, P. Wadley, J. Sinova, D. Kriegner, J. Minár, J. H. Dil, and T. Jungwirth, Altermagnetic lifting of kramers spin degeneracy, *Nature in press* (2023).
 - [11] S. Bhowal and N. A. Spaldin, Magnetic octupoles as the order parameter for unconventional antiferromagnetism, *arXiv:2212.03756* (2022).
 - [12] R. M. Fernandes, V. S. de Carvalho, T. Birol, and R. G. Pereira, Topological transition from nodal to nodeless zeeman splitting in altermagnets, *Arxiv Preprint* (2023).
 - [13] S. Lee, S. Lee, S. Jung, J. Jung, D. Kim, Y. Lee, B. Seok, J. Kim, B. G. Park, L. Šmejkal, C.-J. Kang, and C. Kim, Broken kramers' degeneracy in altermagnetic mnt, *Arxiv Preprint* (2023).
 - [14] C. Wu, K. Sun, E. Fradkin, and S.-C. Zhang, Fermi liquid instabilities in the spin channel, *Physical Review B* **75**, 115103 (2007).
 - [15] R. González-Hernández, L. Šmejkal, K. Výborný, Y. Yahagi, J. Sinova, T. Jungwirth, and J. Železný, Efficient electrical spin splitter based on nonrelativistic collinear antiferromagnetism, *Physical Review Letters* **126**, 127701 (2021).
 - [16] L. Šmejkal, A. B. Hellenes, R. González-Hernández, J. Sinova, and T. Jungwirth, Giant and tunneling magnetoresistance in unconventional collinear antiferromagnets with nonrelativistic spin-momentum coupling, *Physical Review X* **12**, 011028 (2022).
 - [17] K.-H. Ahn, A. Hariki, K.-W. Lee, and J. Kuneš, Antiferromagnetism in ruo 2 as d-wave pomeranchuk instability, *Physical Review B* **99**, 184432 (2019).
 - [18] A. Schofield, There and back again: from magnets to superconductors, *Physics* **2**, 93 (2009).
 - [19] R. Fernandes, A. Chubukov, and J. Schmalian, What drives nematic order in iron-based superconductors?, *Nature physics* **10**, 97 (2014).

- [20] R. Fernandes, A. Chubukov, J. Knolle, I. Eremin, and J. Schmalian, Preemptive nematic order, pseudogap, and orbital order in the iron pnictides, *Physical Review B* **85**, 024534 (2012).
- [21] C.-C. Lee, W.-G. Yin, W. Ku, *et al.*, Ferro-orbital order and strong magnetic anisotropy in the parent compounds of iron-pnictide superconductors, *Physical Review Letters* **103**, 267001 (2009).
- [22] C.-C. Chen, J. Maciejko, A. Sorini, B. Moritz, R. Singh, and T. Devereaux, Orbital order and spontaneous orthorhombicity in iron pnictides, *Physical Review B* **82**, 100504 (2010).
- [23] W. Lv, J. Wu, and P. Phillips, Orbital ordering induces structural phase transition and the resistivity anomaly in iron pnictides, *Physical Review B* **80**, 224506 (2009).
- [24] The Supplemental Material includes (1) a real-space sketch of the orbital tight-binding model, (2) details about the mean-field Hamiltonian, and (3) and extended phase diagram. URL: [url inserted by publisher].
- [25] S. Raghu, X.-L. Qi, C.-X. Liu, D. J. Scalapino, and S.-C. Zhang, Minimal two-band model of the superconducting iron oxypnictides, *Phys. Rev. B* **77**, 220503 (2008).
- [26] J. Kanamori, Superexchange interaction and symmetry properties of electron orbitals, *Journal of Physics and Chemistry of Solids* **10**, 87 (1959).
- [27] M. Daghofer, A. Nicholson, A. Moreo, and E. Dagotto, Three orbital model for the iron-based superconductors, *Physical Review B* **81**, 014511 (2010).
- [28] E. Dagotto, T. Hotta, and A. Moreo, Colossal magnetoresistant materials: the key role of phase separation, *Physics reports* **344**, 1 (2001).
- [29] J. Knolle, I. Eremin, and R. Moessner, Multiorbital spin susceptibility in a magnetically ordered state: Orbital versus excitonic spin density wave scenario, *Physical Review B* **83**, 224503 (2011).
- [30] H. Kim, Y. Yoshida, C.-C. Lee, T.-R. Chang, H.-T. Jeng, H. Lin, Y. Haga, Z. Fisk, and Y. Hasegawa, Atomic-scale visualization of surface-assisted orbital order, *Science advances* **3**, eaao0362 (2017).
- [31] Y. Murakami, J. Hill, D. Gibbs, M. Blume, I. Koyama, M. Tanaka, H. Kawata, T. Arima, Y. Tokura, K. Hirota, *et al.*, Resonant x-ray scattering from orbital ordering in LaMnO_3 , *Physical review letters* **81**, 582 (1998).
- [32] Y. Murakami, H. Kawada, H. Kawata, M. Tanaka, T. Arima, Y. Moritomo, and Y. Tokura, Direct observation of charge and orbital ordering in $\text{La}_{0.5}\text{Sr}_{1.5}\text{MnO}_4$, *Physical review letters* **80**, 1932 (1998).
- [33] T. Mizokawa, D. Khomskii, and G. Sawatzky, Interplay between orbital ordering and lattice distortions in LaMnO_3 , YVO_4 , and YTiO_3 , *Physical Review B* **60**, 7309 (1999).
- [34] I. Mazin, R. González-Hernández, and L. Šmejkal, Induced monolayer altermagnetism in $\text{Mn}(\text{s,se})_3$ and FeSe (2023), arXiv:2309.02355 [cond-mat.mes-hall].
- [35] I. Solovyev, Lattice distortion and magnetism of 3d- t_2g perovskite oxides, *Physical Review B* **74**, 054412 (2006).
- [36] J. B. Goodenough, Magnetism and the chemical bond, (No Title) (1963).
- [37] A. M. Oleś, P. Horsch, L. F. Feiner, and G. Khaliullin, Spin-orbital entanglement and violation of the goodenough-kanamori rules, *Physical review letters* **96**, 147205 (2006).
- [38] W. Geertsma and D. Khomskii, Influence of side groups on 90 superexchange: A modification of the goodenough-kanamori-anderson rules, *Physical Review B* **54**, 3011 (1996).
- [39] G. Khaliullin, Orbital order and fluctuations in mott insulators, *Progress of Theoretical Physics Supplement* **160**, 155 (2005).
- [40] G. Khaliullin, P. Horsch, and A. M. Oleś, Spin order due to orbital fluctuations: Cubic vanadates, *Physical review letters* **86**, 3879 (2001).
- [41] S. Miyasaka, Y. Okimoto, M. Iwama, and Y. Tokura, Spin-orbital phase diagram of perovskite-type RVO_3 (R = rare-earth ion or Y), *Physical Review B* **68**, 100406 (2003).
- [42] C. Ulrich, G. Khaliullin, J. Sirker, M. Reehuis, M. Ohl, S. Miyasaka, Y. Tokura, and B. Keimer, Magnetic neutron scattering study of YVO_3 : Evidence for an orbital peierls state, *Physical review letters* **91**, 257202 (2003).
- [43] H. Meley, M. Tran, J. Teyssier, J. Krieger, T. Prokscha, A. Suter, Z. Salman, M. Viret, D. Van Der Marel, and S. Gariglio, Strain tuning of interorbital correlations in LaVO_3 thin films, *Physical Review B* **103**, 125112 (2021).
- [44] M. Daghofer, A. Nicholson, A. Moreo, and E. Dagotto, Three orbital model for the iron-based superconductors, *Phys. Rev. B* **81**, 014511 (2010).
- [45] V. Leeb, A. Mook, L. Šmejkal, and J. Knolle, Code and data repository: Spontaneous formation of altermagnetism from orbital ordering (2023).

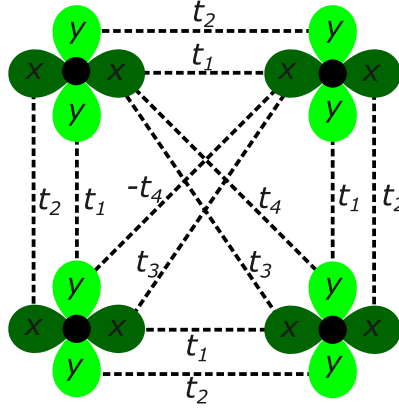


FIG. 4. Visualization of Hamiltonian H_0 . The present hopping terms are shown as dashed lines between the x and y orbital.

SUPPLEMENTARY MATERIAL

Appendix A: Model and Hamiltonian

We show the hopping structure of the non-interacting part of the Hamiltonian H_0 in Fig. 4. Fourier transformation leads to Eq. (1) [25].

After mean-field decoupling we obtain $H = \sum_{\mathbf{k}} \Psi_{\mathbf{k}}^\dagger h(\mathbf{k}) \Psi_{\mathbf{k}} + E_0$ with

$$h(\mathbf{k}) = \mathbb{1} \otimes T(\mathbf{k}) - 16J\delta m(\tau^z \otimes \tau^z \otimes \mathbb{1}) - 16V\delta n(\tau^z \otimes \mathbb{1} \otimes \tau^z) \quad (\text{A1})$$

and $T(\mathbf{k})$ is a 4×4 matrix with

$$\begin{aligned} T_{11}(\mathbf{k}) &= T_{22}(\mathbf{k}) = T_{33}(\mathbf{k}) = T_{44}(\mathbf{k}) = -2t_3(\cos(k_x + k_y) + \cos(k_x - k_y)) - \mu \\ T_{12}(\mathbf{k}) &= T_{21}(\mathbf{k}) = T_{43}(\mathbf{k}) = T_{34}(\mathbf{k}) = -2t_4(\cos(k_x + k_y) - \cos(k_x - k_y)) \\ T_{13}(\mathbf{k}) &= T_{31}(\mathbf{k})^* = -t_1(1 + e^{2ik_x}) - 2t_2e^{ik_x} \cos(k_y) \\ T_{24}(\mathbf{k}) &= T_{42}(\mathbf{k})^* = -t_2(1 + e^{2ik_x}) - 2t_1e^{ik_x} \cos(k_y) \end{aligned} \quad (\text{A2})$$

in the basis $(\Psi_{\mathbf{k}xA\uparrow}, \Psi_{\mathbf{k}yA\uparrow}, \Psi_{\mathbf{k}xB\uparrow}, \Psi_{\mathbf{k}yB\uparrow}, \Psi_{\mathbf{k}xA\downarrow}, \Psi_{\mathbf{k}yA\downarrow}, \Psi_{\mathbf{k}xB\downarrow}, \Psi_{\mathbf{k}yB\downarrow})$ and the energy constant $E_0 = 64J\delta m^2 + 64V\delta n^2$. Note that τ^z is the Pauli- z matrix.

Appendix B: Full phase diagram

In principle our model has at least four different tunable parameters, i.e. the interactions J, V , temperature and the filling n . Based on the well understood effect of the interactions, we do not expect to find any additional instabilities in the phase diagram. For completeness, we show the phase diagram and the spin conductivity σ^z for various fillings n and interaction strengths, but fixed interaction ratio $J = V$ in Fig. 5.

We observe that the presence of OO and AFM order as well as their coexistence is generic for any filling. OO is dominant at half filling whereas AFM order features its minimal critical interaction around quarter and three quarter filling. Large regions of the phase diagram are again dominated by the coexistence of OO and AFM, i.e. the altermagnetic phase. At exactly half filling an insulator forms which is expected to become extended for more generic Hubbard-like interactions.

For finite temperatures we found rather conventional behavior, i.e. the two different critical interaction strengths decrease with increasing temperature, leading to two independent critical temperatures.

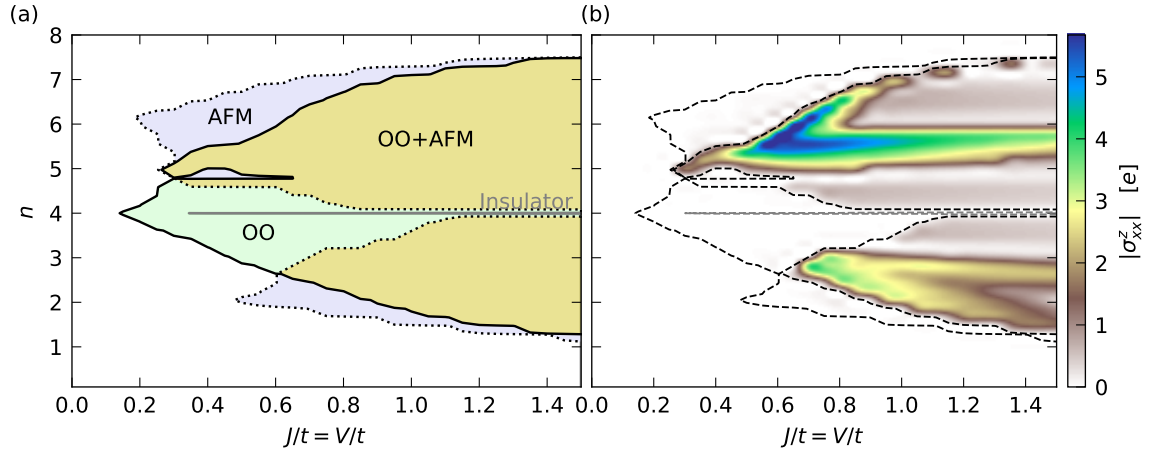


FIG. 5. (a) Phase diagram for various fillings n and $V = J$. At half filling an OO insulator emerges. The altermagnetic phase, where OO and AFM order coexist, is always a metal. (b) Colorplot of the spin conductivity σ_{xx}^z . The phase boundaries of (a) are shown as dashed lines.